JOURNAL OF MAGNETIC RESONANCE **124,** 459–467 (1997)
ARTICLE NO. MN961070

Doubly Sensitivity-Enhanced 3D HCCH-TOCSY of ^{13}C-Labeled Proteins in H_2O Using Heteronuclear Cross Polarization and Pulsed Field Gradients

SYBREN S. WIJMENGA,*,†,‡ ELLES STEENSMA,§ AND CARLO P. M. VAN MIERLO§

*Nijmegen SON Research Center for Molecular Design, Structure and Synthesis, SON/NWO National HF-NMR Facility, Toernooiveld 6525 ED Nijmegen, The Netherlands; and §Department of Biochemistry, Wageningen Agricultural University, Wageningen, The Netherlands

Received September 10, 1996

Singly and doubly sensitivity-enhanced versions are described of the three-dimensional cross-polarization driven HCCH–TOCSY experiment (3D CP HCCH–TOCSY), which employ enhanced cross-polarization sequences with gradient coherence selection for both the $^1H \rightarrow {}^{13}C$ transfer step and the $^{13}C \rightarrow {}^1H$ transfer step. The sequences are demonstrated on a $^{13}C/^{15}N$ doubly labeled sample of flavodoxin II of *Azotobacter vinelandii* (179 amino acid residues; 20 kDa) dissolved in 90% H_2O/10% D_2O. The presented implementations of 3D CP HCCH–TOCSY experiments are simple and robust with regard to missettings and therefore easy to use and set up.

The assignment of resonances of larger biomolecules requires a combination of several multidimensional heteronuclear experiments [see, for example, (*1, 2*)]. The generally used protocol is to obtain main-chain resonance assignments from three-dimensional triple-resonance experiments and to subsequently extract the side-chain resonances from 3D HCCH–COSY or 3D HCCH–TOCSY experiments [see, for example, (*1*)]. Originally, the 3D HCCH–TOCSY experiment was based on INEPT (RINEPT) sequences (*3, 4*). Since the 3D HCCH–TOCSY experiments are essential for the assignment procedure, improved implementations are of major importance. The cross-polarization driven HCCH–TOCSY experiment, in which the $^1H \rightarrow {}^{13}C$ and $^{13}C \rightarrow {}^1H$ magnetization transfers are accomplished via heteronuclear cross polarization (*5–7*), is such an improvement. First, heteronuclear cross polarization, CP, is more effective with regard to the $^1H \rightarrow {}^{13}C$ and $^{13}C \rightarrow {}^1H$ magnetization transfers then INEPT(RINEPT) (*6*). Second, to avoid chemical-shift changes associated with isotope effects and with sample handling, it is desirable to use one $^{13}C/^{15}N$-labeled sample dissolved in H_2O for both the triple-resonance and the HCCH–TOCSY experiments. The CP HCCH–TOCSY sequence (*7*) which employs B_0 field gradients as spoiling pulses to suppress the water signal shows good H_2O suppression, and therefore allows CP HCCH–TOCSY experiments to be recorded in H_2O.

The CP HCCH–TOCSY sequence introduced by Wang and Zuiderweg (*7*) does not select coherence pathways via the use of gradients; instead, the artifacts are suppressed via conventional phase cycling and the use of trim pulses. However, it has now been recognized that coherence-pathway selection via gradients is the foremost method to suppress artifacts and to obtain excellent water suppression (*8*). In addition, when coherence-pathway selection via gradients is used in combination with an enhanced INEPT sequence, eINEPT, an increase in sensitivity of a factor of $2^{1/2}$ per individual transfer step can be achieved (*9*). Single enhancement of the final transfer step by an eINEPT sequence is now routinely applied in 2D and 3D NMR experiments (*8*). However, the sensitivity improvement in *n*D NMR experiments can be as high as $2^{(n-1)1/2}$, when each transfer step in the *n*D experiment is modified into an enhanced sequence (*10, 11*). Double enhancement using eINEPT sequences has been demonstrated in a number of 3D NMR experiments (*10–13*).

Since the cross-polarization sequence can be modified into an enhanced sequence (*14*), sensitivity improvements of the 3D CP HCCH–TOCSY experiment are also possible. The double-enhancement approach has been demonstrated in a 3D HCCH–TOCSY experiment by Sattler *et al.* (*10, 11*), in which an enhanced CP sequence transfers magnetization from $^1H \rightarrow {}^{13}C$ and an e(R)INEPT sequence transfers magnetization from $^{13}C \rightarrow {}^1H$. Considerable sensitivity improvement as compared to the singly enhanced and unenhanced versions of the experiments were obtained. Sattler *et al.* (*11*) also noted good water suppression, given their gradient and pulse settings, but did not discuss the water suppression method in detail.

No singly or doubly sensitivity-enhanced versions of 3D CP HCCH–TOCSY experiments have been tested, in which

† To whom correspondence should be addressed.
‡ Present address: Department of Medical Biophysics, Umeå University, S-901 87 Umeå, Sweden.

1090-7807/97 $25.00

both the $^1H \rightarrow {}^{13}C$ and the $^{13}C \rightarrow {}^1H$ transfer steps employ cross-polarization sequences. Here, we present such sequences which have a considerably improved sensitivity as compared to the already quite sensitive conventional 3D CP HCCH–TOCSY sequence (*7*). The extremely good water suppression achieved by these sequences results in the observation of undisturbed cross peaks directly on the water line. A simple but robust protocol is derived to obtain this degree of suppression. Consequently, the previous necessity to acquire 3D HCCH–TOCSY experiments in D_2O is avoided.

Figure 1A shows a slightly modified version of the unenhanced CP HCCH–TOCSY sequence as originally proposed by Wang and Zuiderweg (*7*). The singly and doubly enhanced version of the 3D CP HCCH–TOCSY pulse sequences as proposed by us are shown in Figs. 1B and 1C, respectively.

In the standard unenhanced CP HCCH–TOCSY experiment (Fig. 1A), source-proton magnetization frequency labeled in t_1 is transferred to its covalently attached ^{13}C nucleus over the one-bond scalar coupling via heteronuclear cross polarization. The resulting in-phase ^{13}C magnetization is frequency labeled in t_2 and subsequently transferred to other carbons in the same residue through a homonuclear TOCSY transfer. Finally, the ^{13}C magnetization is transferred via another heteronuclear CP sequence to the destination proton and detected (*7*). Both the cos- and sine-modulated signals must be measured to obtain sign discrimination in F_1 and F_2 (*15*). Finally, following the conventions as used by van de Ven (*16*), four possible terms arise for the detectable signal,

$$\sigma^{cc} = i\tfrac{1}{2}H^{-}\cos(\omega_H t_1)\cos(\omega_C t_2) \quad (\text{with } \phi_0 = x;\ \phi_3 = y) \qquad [1a]$$

$$\sigma^{cs} = i\tfrac{1}{2}H^{-}\cos(\omega_H t_1)\sin(\omega_C t_2) \quad (\text{with } \phi_0 = x;\ \phi_3 = -x) \qquad [1b]$$

$$\sigma^{sc} = i\tfrac{1}{2}H^{-}\sin(\omega_H t_1)\cos(\omega_C t_2) \quad (\text{with } \phi_0 = y;\ \phi_3 = y) \qquad [1c]$$

$$\sigma^{ss} = i\tfrac{1}{2}H^{-}\sin(\omega_H t_1)\sin(\omega_C t_2) \quad (\text{with } \phi_0 = y;\ \phi_3 = -x). \qquad [1d]$$

Three-dimensional Fourier transformation of the amplitude-modulated H^- coherences leads to pure-absorption-mode cross peaks with sign discrimination in F_1 and F_2. For a detailed description of unwanted pathways, we refer to Majumdar *et al.* (*6*). Water suppression in this standard sequence (Fig. 1A) is achieved by the use of B_0 field gradients which act as strong homospoil pulses while the ^{13}C magnetization of interest is placed along the *z* axis, as described by Wang and Zuiderweg (*7*).

In the singly enhanced version of the experiment (Fig.

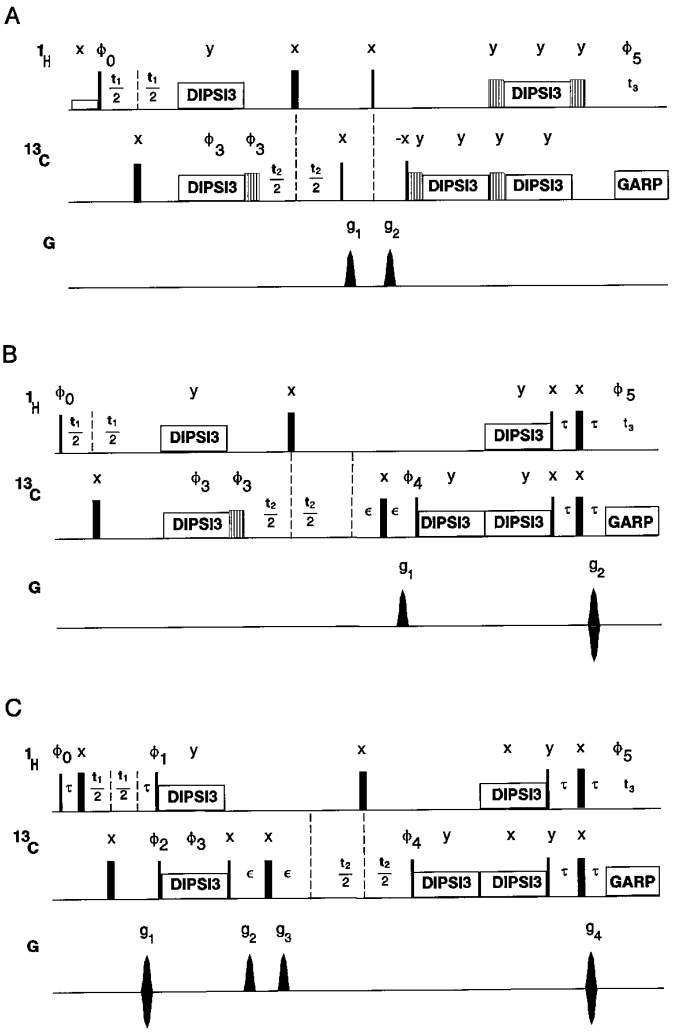

FIG. 1. Pulse sequences for the 3D CP HCCH–TOCSY experiment. Narrow and wide pulses represent 90° and 180° flip angles, respectively. All B_0-field gradients are sine-bell shaped. The heteronuclear and homonuclear cross polarizations were carried out using synchronous DIPSI3 sequences (*18*). The trim pulses bracketing the DIPSI3 sequences are indicated by vertical lines. Carbon decoupling during acquisition is achieved via a GARP sequence (*20*). (A) Standard nonenhanced pulse sequence (*7*). The phase cycle used is $\phi_0 = x$; $\phi_3 = y, -y$; $\phi_5 = x, -x$. Quadrature detection in the t_1 and the t_2 dimension is obtained by using the States–TPPI method (*1, 2, 19*) in which the phases ϕ_0 and ϕ_3 are separately incremented. Optional presaturation during the relaxation delay is indicated by an open box. (B) Singly enhanced pulse sequence. The phase cycle used is $\phi_0 = x$; $\phi_3 = y, -y$; $\phi_4 = x$; $\phi_5 = x, -x$. Quadrature detection in the t_1 dimension is obtained via the States–TPPI method by incrementing phase ϕ_0. Absorption-mode spectra in the t_2 dimension are obtained by separate measurements of the N- and P-type coherences, which is achieved by simultaneously inverting the sign of gradient g_2 and of phase ϕ_4. (C) Doubly enhanced pulse sequence. The phase cycle used is $\phi_0 = y$, $\phi_1 = x$; $\phi_2 = x, -x$; $\phi_3 = y$; $\phi_4 = y$; $\phi_5 = x, -x$. Absorption-mode spectra in the indirect dimensions are obtained by separate measurements of the N- and P-type coherences, which is achieved by simultaneously inverting the sign of gradient g_1 and of phase ϕ_1 for the t_1 dimension and by simultaneously inverting the sign of gradient g_4 and of phase ϕ_4 for the t_2 dimension.

The values to be used for delay lengths, gradient amplitudes, gradient durations, and field strengths are given in the legends to Figs. 2 and 3, respectively.

1B), the homonuclear carbon TOCSY sequence followed by the heteronuclear CP sequence is replaced by its enhanced counterpart (eTOCSY–eCP). As in sequence 1A, the t_1-labeled in-phase proton magnetization is transferred to in-phase ^{13}C magnetization via a heteronuclear CP sequence. During t_2, the ^{13}C magnetization is frequency labeled. The subsequent transfer to other carbons in the same residue followed by transfer to the destination proton is accomplished by an eTOCSY–eCP sequence. This sequence consists of consecutive homonuclear carbon TOCSY and heteronuclear CP sequences, bracketed in the front by a ^{13}C $90^\circ_{\phi 4}$ pulse and in the back by two simultaneous ^1H 90°_x and ^{13}C 90°_x pulses. The homonuclear TOCSY sequence is isotropic and transfers C_x, C_y, and C_z equally well. The CP sequence is described by a planar Hamiltonian (*14*). Via some tedious but straightforward operator algebra it can be derived that the eTOCSY–eCP sequence followed by a τ—180°—τ period transfers $C^+ \rightarrow H^+$ and $C^- \rightarrow H^-$ when $\phi_4 = x$ and transfers $C^+ \rightarrow H^-$ and $C^- \rightarrow H^+$ when $\phi_4 = -x$. Finally, four possible terms arise in the singly enhanced 3D CP HCCH–TOCSY sequence (Fig. 1B),

$$\sigma^{cN} = +\tfrac{1}{2}iH^+\cos(\omega_H t_1)e(+i\gamma_C g_1\tau_1 + i\gamma_H g_2\tau_2 - i\omega_C t_2) - \tfrac{1}{2}iH^-\cos(\omega_H t_1)e(-i\gamma_C g_1\tau_1 - i\gamma_H g_2\tau_2 + i\omega_C t_2)$$
(with $\phi_0 = x$; $\phi_4 = x$, N-type) [2a]

$$\sigma^{cP} = +\tfrac{1}{2}iH^-\cos(\omega_H t_1)e(+i\gamma_C g_1\tau_1 - i\gamma_H g_2\tau_2 - i\omega_C t_2) - \tfrac{1}{2}iH^+\cos(\omega_H t_1)e(-i\gamma_C g_1\tau_1 + i\gamma_H g_2\tau_2 + i\omega_C t_2)$$
(with $\phi_0 = x$; $\phi_4 = -x$, P-type) [2b]

$$\sigma^{sN} = +\tfrac{1}{2}iH^+\sin(\omega_H t_1)e(+i\gamma_C g_1\tau_1 + i\gamma_H g_2\tau_2 - i\omega_C t_2) - \tfrac{1}{2}iH^-\sin(\omega_H t_1)e(-i\gamma_C g_1\tau_1 - i\gamma_H g_2\tau_2 + i\omega_C t_2)$$
(with $\phi_0 = y$; $\phi_4 = x$, N-type) [2c]

$$\sigma^{sP} = +\tfrac{1}{2}iH^-\sin(\omega_H t_1)e(+i\gamma_C g_1\tau_1 - i\gamma_H g_2\tau_2 - i\omega_C t_2) - \tfrac{1}{2}iH^+\sin(\omega_H t_1)e(-i\gamma_C g_1\tau_1 + i\gamma_H g_2\tau_2 + i\omega_C t_2)$$
(with $\phi_0 = y$; $\phi_4 = -x$, P-type). [2d]

Only the H^- terms lead to detectable signal. Proper linear combination of the N-type and P-type signals gives the amplitude-modulated signals,

$$\sigma^{cN} - \sigma^{cP} = -iH^-\cos(\omega_H t_1)\cos(\omega_C t_2) \quad [3a]$$

$$\sigma^{cN} + \sigma^{cP} = 1\ H^-\cos(\omega_H t_1)\sin(\omega_C t_2) \quad [3b]$$

$$\sigma^{sN} - \sigma^{sP} = -iH^-\sin(\omega_H t_1)\cos(\omega_C t_2) \quad [3c]$$

$$\sigma^{sN} + \sigma^{sP} = 1\ H^-\sin(\omega_H t_1)\sin(\omega_C t_2). \quad [3d]$$

The terms [3b] and [3d] are 90° out of phase with respect to the corresponding terms obtained using the conventional sequence 1A, terms [1b] and [1d], as follows from the absence of the imaginary number i. Correct phases are obtained by interchanging the imaginary and real parts of their FIDs and negating the imaginary parts of the resulting FIDs. Subsequent Fourier transformation leads then to absorption-mode peaks with frequency discrimination in F_1 and F_2.

The difference between the conventional experiment and the experiment employing gradients for coherence-pathway selection is that the separately measured N- and P-type signals must be added or subtracted for the latter experiment (compare Eqs. [1a]–[1d] with [3a]–[3d]). This procedure leads to an averaging of the noise by a factor of $2^{1/2}$. Hence, whereas the signal increases by a factor of 2 in the enhanced experiment, the ultimate signal-to-noise ratio increases only by a factor of $2^{1/2}$ (i.e., 2 divided by $2^{1/2}$) as compared to the conventional experiment. Note that per free-induction decay the same signal amplitudes are obtained in the conventional unenhanced and singly enhanced versions of the 3D experiment (compare Eqs. [1a]–[1d] with [2a]–[2d]). Thus for testing purposes, the singly enhanced sequence 1B gives the same signal amplitude as the unenhanced sequence 1A for $t_1 = 0$ and $t_2 = 0$.

To select a specific coherence pathway, the corresponding net phase resulting from the gradients incorporated into the pulse sequence must be zero (see Eqs. [2a]–[2d]). We have decided to keep both the gradient amplitudes and lengths constant: $|g_2|\tau_2 = +(\gamma_H/\gamma_C)|g_1|\tau_1$. Consequently, coherence-pathway selection of the four different routes can be achieved by simply permuting the sign of the last gradient,

$$\text{cN: s}(+, -) \quad [4a]$$

$$\text{cP: s}(+, +) \quad [4b]$$

$$\text{sN: s}(+, -) \quad [4c]$$

$$\text{sP: s}(+, +). \quad [4d]$$

As the product of amplitude and length of the first gradient is considerably larger than that of the last gradient, unwanted residual ^1H coherences corresponding to protons

not bound to ^{13}C atoms, such as those from H_2O, are dephased. Because the change of the gradient sign necessary for coherence-pathway selection takes place on the relatively weak and short last gradient in the pulse sequence, the variation in total defocusing of such unwanted coherences is rather limited.

In the doubly enhanced version of the 3D CP HCCH–TOCSY experiment (Fig. 1C), both the first CP sequence and the TOCSY–CP sequence are replaced by their enhanced counterparts, the eCP sequence and the eTOCSY–eCP sequence, respectively. In the doubly enhanced sequence (Fig. 1C), the source proton magnetization is frequency labeled during t_1. In addition, during the two τ periods, anti-phase proton magnetization develops, which is dephased by the first gradient. Subsequently, the eCP sequence, which consists of the CP sequence bracketed in the front by simultaneous $^1H\ 90^\circ_{\phi 1}$ and $^{13}C\ 90^\circ_{\phi 2}$ pulses and in the back by a $^{13}C\ 90^\circ_x$ pulse, transfers $iH^-C_z \rightarrow \frac{1}{2}C^+$ and $-iH^+C_z \rightarrow \frac{1}{2}C^-$, when $\phi_1 = x$, and $-iH^-C_z \rightarrow \frac{1}{2}C^-$ and $iH^+C_z \rightarrow \frac{1}{2}C^+$, when $\phi_1 = -x$. After the application of the rephasing gradient g_2 and dephasing gradient g_3, the C^+ and C^- coherences are ^{13}C-frequency labeled during t_2. The eTOCSY–eCP sequence followed by the τ—180°—τ period transfers $C^+ \rightarrow -H^+$ and $C^- \rightarrow -H^-$, when $\phi_4 = y$ and $C^+ \rightarrow H^-$ and $C^- \rightarrow H^+$, when $\phi_4 = -y$. Finally, four possible terms arise in the doubly enhanced 3D CP HCCH–TOCSY sequence,

$$\sigma^{NN} = +\tfrac{1}{2}H^-e(-i\omega_H t_1 - i\gamma_H g_1\tau_1 - i\gamma_C g_2\tau_2 + i\gamma_C g_3\tau_3 - i\gamma_H g_4\tau_4 + i\omega_C t_2)$$
$$+ \tfrac{1}{2}H^+e(+i\omega_H t_1 + i\gamma_H g_1\tau_1 + i\gamma_C g_2\tau_2 - i\gamma_C g_3\tau_3 + i\gamma_H g_4\tau_4 - i\omega_C t_2)$$
$$(\text{with } \phi_1 = -x, \text{ N-type; } \phi_4 = -y, \text{ N-type}) \quad [5a]$$

$$\sigma^{NP} = -\tfrac{1}{2}H^+e(-i\omega_H t_1 - i\gamma_H g_1\tau_1 - i\gamma_C g_2\tau_2 + i\gamma_C g_3\tau_3 + i\gamma_H g_4\tau_4 + i\omega_C t_2)$$
$$- \tfrac{1}{2}H^-e(+i\omega_H t_1 + i\gamma_H g_1\tau_1 + i\gamma_C g_2\tau_2 - i\gamma_C g_3\tau_3 - i\gamma_H g_4\tau_4 - i\omega_C t_2)$$
$$(\text{with } \phi_1 = -x, \text{ N-type; } \phi_4 = y, \text{ P-type}) \quad [5b]$$

$$\sigma^{PN} = -\tfrac{1}{2}H^+e(-i\omega_H t_1 - i\gamma_H g_1\tau_1 + i\gamma_C g_2\tau_2 - i\gamma_C g_3\tau_3 + i\gamma_H g_4\tau_4 - i\omega_C t_2)$$
$$- \tfrac{1}{2}H^-e(+i\omega_H t_1 + i\gamma_H g_1\tau_1 - i\gamma_C g_2\tau_2 + i\gamma_C g_3\tau_3 - i\gamma_H g_4\tau_4 + i\omega_C t_2)$$
$$(\text{with } \phi_1 = x, \text{ P-type; } \phi_4 = -y, \text{ N-type}) \quad [5c]$$

$$\sigma^{PP} = +\tfrac{1}{2}H^-e(-i\omega_H t_1 - i\gamma_H g_1\tau_1 + i\gamma_C g_2\tau_2 - i\gamma_C g_3\tau_3 - i\gamma_H g_4\tau_4 - i\omega_C t_2)$$
$$+ \tfrac{1}{2}H^+e(+i\omega_H t_1 + i\gamma_H g_1\tau_1 - i\gamma_C g_2\tau_2 + i\gamma_C g_3\tau_3 + i\gamma_H g_4\tau_4 + i\omega_C t_2)$$
$$(\text{with } \phi_1 = x, \text{ P-type; } \phi_4 = y, \text{ P-type}). \quad [5d]$$

FIG. 2. Two-dimensional initial planes ($t_1 = 0$ or $t_2 = 0$) from 3D CP HCCH–TOCSY spectra obtained by using the pulse sequences of Fig. 1 on a 5 m*M* uniformly $^{13}C/^{15}N$-labeled flavodoxin sample in 90% H_2O/10% D_2O. Planes (A, B) demonstrate the effect on the CP HCCH–TOCSY experiment of enhancement in the t_2 dimension. (A) $^{13}C-^1H$ plane recorded with the standard pulse sequence 1A ($t_1 = 0$); the amplitudes of gradients g_1 and g_2 are 40 (with 100 corresponding to 60 G/cm), and their durations are 4 and 1 ms, respectively. (B) $^{13}C-^1H$ plane recorded with the singly enhanced pulse sequence 1B ($t_1 = 0$); the amplitudes of gradients g_1 and g_2 are 80 and 40, respectively, and the corresponding gradient durations are 0.5 and 0.25 ms. Planes (C, D) demonstrate the effect on the CP HCCH–TOCSY experiment of enhancement of the t_1 dimension as well. (C) $^1H-^1H$ plane recorded with the singly enhanced pulse sequence 1B ($t_2 = 0$); the amplitudes of gradients g_1 and g_2 are 80 and 40, respectively, and the corresponding gradient durations are 0.5 and 0.25 ms. (D) $^1H-^1H$ plane recorded with the doubly enhanced pulse sequence 1C ($t_2 = 0$); the amplitudes of gradients g_1 to g_4 are 20, 40, 80, and 40, respectively, and the corresponding gradient durations are 0.25, 0.5, 0.5, and 0.25 ms.

All spectra were acquired on a Bruker AMX2 600 spectrometer equipped with a triple-resonance probe head with a doubly tuned {^1H, ^{13}C} inner coil, a broadband outer coil, and a self-shielded *z*-gradient coil. The spectra were recorded with the following settings: the ^1H and ^{13}C carrier positions at the H_2O resonance frequency and at 43.5 ppm, respectively; spectral widths of 9615 Hz in the ^1H dimensions and 10,571 Hz in the ^{13}C dimension; 512 and 128 complex points in the ^1H acquisition and ^1H indirect dimension, respectively, and 98 complex points in the ^{13}C dimension; 32 FIDs were accumulated per increment; 0.7 s relaxation delay between scans; carbon decoupling during acquisition was achieved via a GARP sequence (*20*) with a 3.6 kHz RF field; the delays τ and ϵ were set to 1.55 and 0.75 ms, respectively; the heteronuclear and homonuclear cross polarizations were carried out using synchronous DIPSI3 sequences (*18*) with RF field strengths of 9.5 kHz; when present the trim pulses were of 1 ms duration; in the case of (A), a weak presaturation field of approximately 2.5 Hz was applied during the relaxation delay. All data were identically processed. Prior to Fourier transformation, the FIDs were multiplied by a quadratic cosine filter in both dimensions and zero filled. Only positive levels are shown; planes (A, B) are plotted at identical levels, as are planes (C, D).

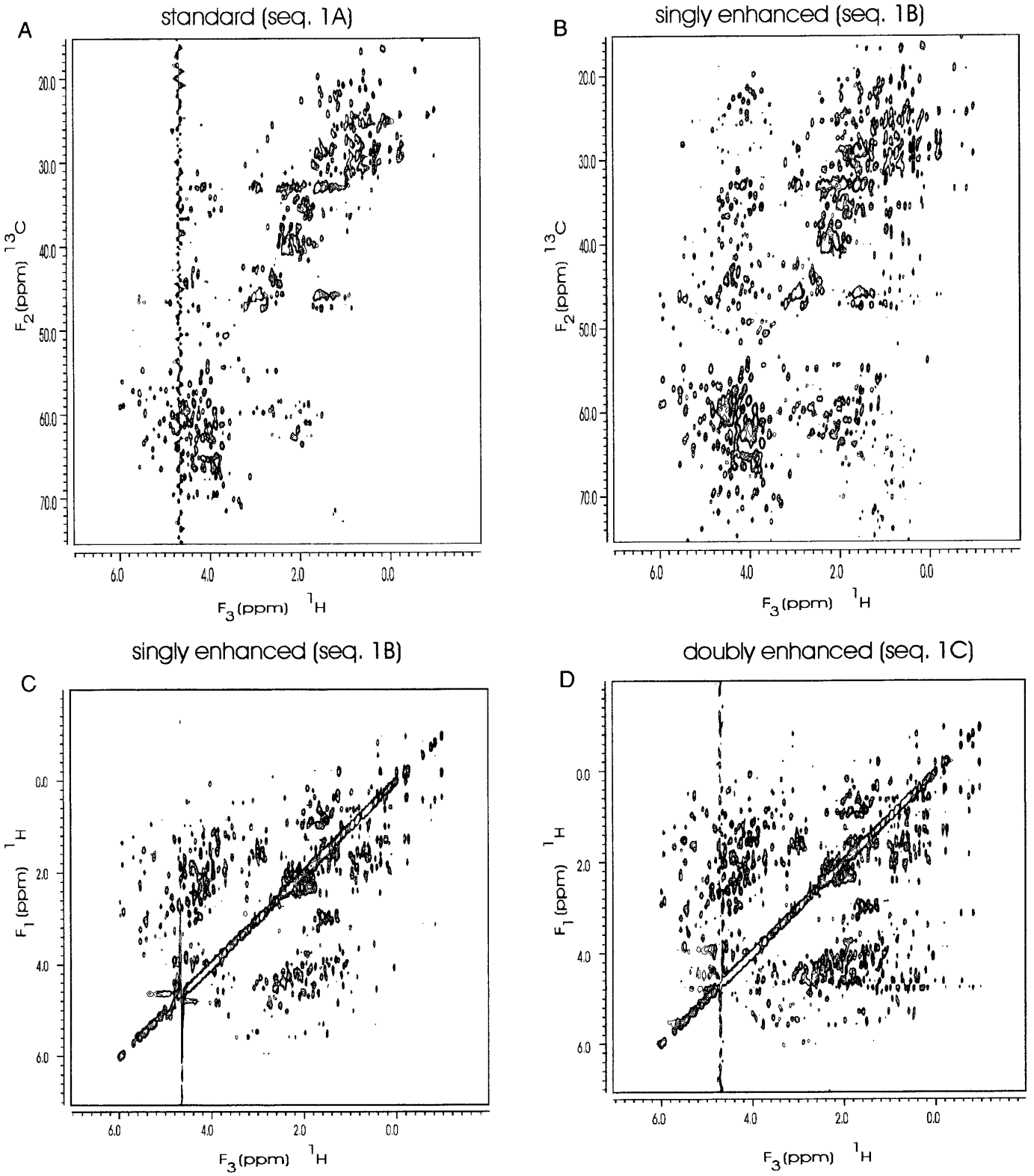
A
standard (seq. 1A)
B
singly enhanced (seq. 1B)
C
singly enhanced (seq. 1B)
D
doubly enhanced (seq. 1C)
F2 (ppm) 13C
F3 (ppm) 1H
F1 (ppm) 1H
20.0
30.0
40.0
50.0
60.0
70.0
0.0
2.0
4.0
6.0

FIGURE 2

Only the H^- terms will lead to detectable signal. Amplitude-modulated detectable H^- coherences can be obtained via proper linear combinations of the σ terms,

$$\sigma^{NN} - \sigma^{NP} - \sigma^{PN} + \sigma^{PP} = +2H^-\cos(\omega_H t_1)\cos(\omega_C t_2) \quad [6a]$$

$$\sigma^{NN} + \sigma^{NP} - \sigma^{PN} - \sigma^{PP} = +2iH^-\cos(\omega_H t_1)\sin(\omega_C t_2) \quad [6b]$$

$$\sigma^{NN} + \sigma^{NP} + \sigma^{PN} + \sigma^{PP} = -2iH^-\sin(\omega_H t_1)\cos(\omega_C t_2) \quad [6c]$$

$$\sigma^{NN} - \sigma^{NP} + \sigma^{PN} - \sigma^{PP} = +2H^-\sin(\omega_H t_1)\sin(\omega_C t_2). \quad [6d]$$

The signal amplitude is now four times as large as that obtained for the conventional unenhanced 3D CP HCCH–TOCSY sequence (compare Eqs. [1a]–[1d] with [6a]–[6d]). As discussed before, the required addition and subtraction procedure leads to an averaging of the noise, here by a factor of $4^{1/2}$. Hence, although the signal increases by a factor of 4 in this doubly enhanced, as compared to the conventional unenhanced, experiment, the ultimate signal-to-noise ratio increases only by a factor of 2 (i.e., 4 divided by $4^{1/2}$). Three-dimensional Fourier transformation of the amplitude-modulated H^- coherences leads to pure-absorption-mode cross peaks with sign discrimination in F_1 and F_2. Finally, note that per individual free-induction-decay identical signal amplitudes are obtained for the conventional unenhanced, the singly enhanced, and the doubly enhanced versions of the 3D experiment (compare Eqs. [1a]–[1d], [2a]–[2d], and [5a]–[2d]), when $t_1 = 0$ and $t_2 = 0$.

To select a specific coherence pathway, the corresponding net phase resulting from the gradients incorporated into the pulse sequence must be zero (see Eqs. [5a]–[5d]). Since four gradients are used, a certain element of freedom remains to achieve the desired coherence-pathway selection. Both the number of gradients used, as well as their length or amplitude may be altered. Only one gradient during the t_2 evolution period would suffice for coherence-pathway selection in both the t_1 and the t_2 evolution period. However, we have chosen to use two gradients during the t_2 evolution period. This has the advantage that one can achieve coherence-pathway selection for each of the two transfer steps independently and thereby test the quality of each individual selection step. We have decided to keep both the gradient amplitudes and lengths constant: $|g_2|\tau_2 = +(\gamma_H/\gamma_C)|g_1|\tau_1$ and $|g_3|\tau_3 = +(\gamma_H/\gamma_C)|g_4|\tau_4$. Consequently, coherence-pathway selection of the four different routes can be achieved by simply permutating the signs of the first and last gradient,

$$\text{NN: } s(-, +, +, +) \quad [7a]$$

$$\text{NP: } s(-, +, +, -) \quad [7b]$$

$$\text{PN: } s(+, +, +, +) \quad [7c]$$

$$\text{PP: } s(+, +, +, -). \quad [7d]$$

The strong second and third gradients deliberately have the same sign, as this results in additive defocusing of unwanted residual ^1H coherences corresponding to protons not bound to ^{13}C atoms. This is of crucial importance for the suppression of the water signal. As the change of gradient signs necessary for coherence-pathway selection takes place on the relatively weak and short first and last gradients in the pulse sequence, the resulting variation in total defocusing of the unwanted coherences is limited.

A potential drawback of the use of enhanced coherence-transfer sequences is that they tend to be longer then the corresponding unenhanced versions and that they require additional pulses, which both may lead to signal loss. In the case of the 3D CP HCCH–TOCSY sequence, however, incorporation of the enhanced transfer sequences into the standard CP HCCH–TOCSY sequence does not require a substantially larger number of additional pulses and delays. The total lengthening of the doubly enhanced sequence (Fig. 1C) as compared to the standard unenhanced sequence (Fig. 1A) is only $4\tau + 2\epsilon - 4$ trim = 6.2 ms + 1.5 ms − 4 ms = 3.7 ms (delay durations as given in Fig. 2). Thus, no significant extra signal loss due to T_2 relaxation is expected.

To establish the sensitivity improvement achieved by the

FIG. 3. Doubly enhanced 3D CP HCCH–TOCSY spectrum obtained with sequence 1C on a 5 m*M* uniformly $^{13}C/^{15}N$-labeled flavodoxin sample in 90% H_2O/10% D_2O. An arrow marks the position of the H_2O resonance. (A) Region of the $^1H-^1H$ plane at $F_2 = 53.9$ ppm with a H_α diagonal cross peak at the H_2O resonance. (B) Region of the $^1H-^1H$ plane at $F_2 = 22.2$ ppm with a H_α cross peak near the H_2O resonance. (C) One-dimensional slice through $F_1 = 4.7$ ppm and $F_2 = 53.9$ ppm. (D) One-dimensional slice through $F_1 = 1.0$ ppm and $F_2 = 22.2$ ppm. The 3D spectrum was acquired on a Bruker AMX2 600 spectrometer equipped with a four-resonance probe head with a doubly tuned {^1H, ^{31}P} inner coil, a doubly tuned {^{13}C, ^{15}N} outer coil, and a self-shielded *XYZ*-gradient coil. All settings were as described in the legend to Fig. 2, except for the following changes: 128, 64, and 512 complex points were acquired in the t_1, t_2, and t_3 dimensions, respectively; four FIDs were accumulated per increment; the amplitudes of gradients g_1 to g_4 were 30, 60, 80, and 40, respectively, and the corresponding gradient durations were 1, 2, 2, and 1 ms; the delay ϵ was set to 2.25 ms; Lorentzian to Gaussian transformation and squared shifted-sine bell window functions were applied in the direct and indirect dimensions, respectively. The final frequency matrix consists of 256, 128, and 1024 real points in the F_1, F_2, and F_3 dimensions, respectively. Figures (A, B) are plotted at identical positive levels; figures (C, D) are plotted full scale.

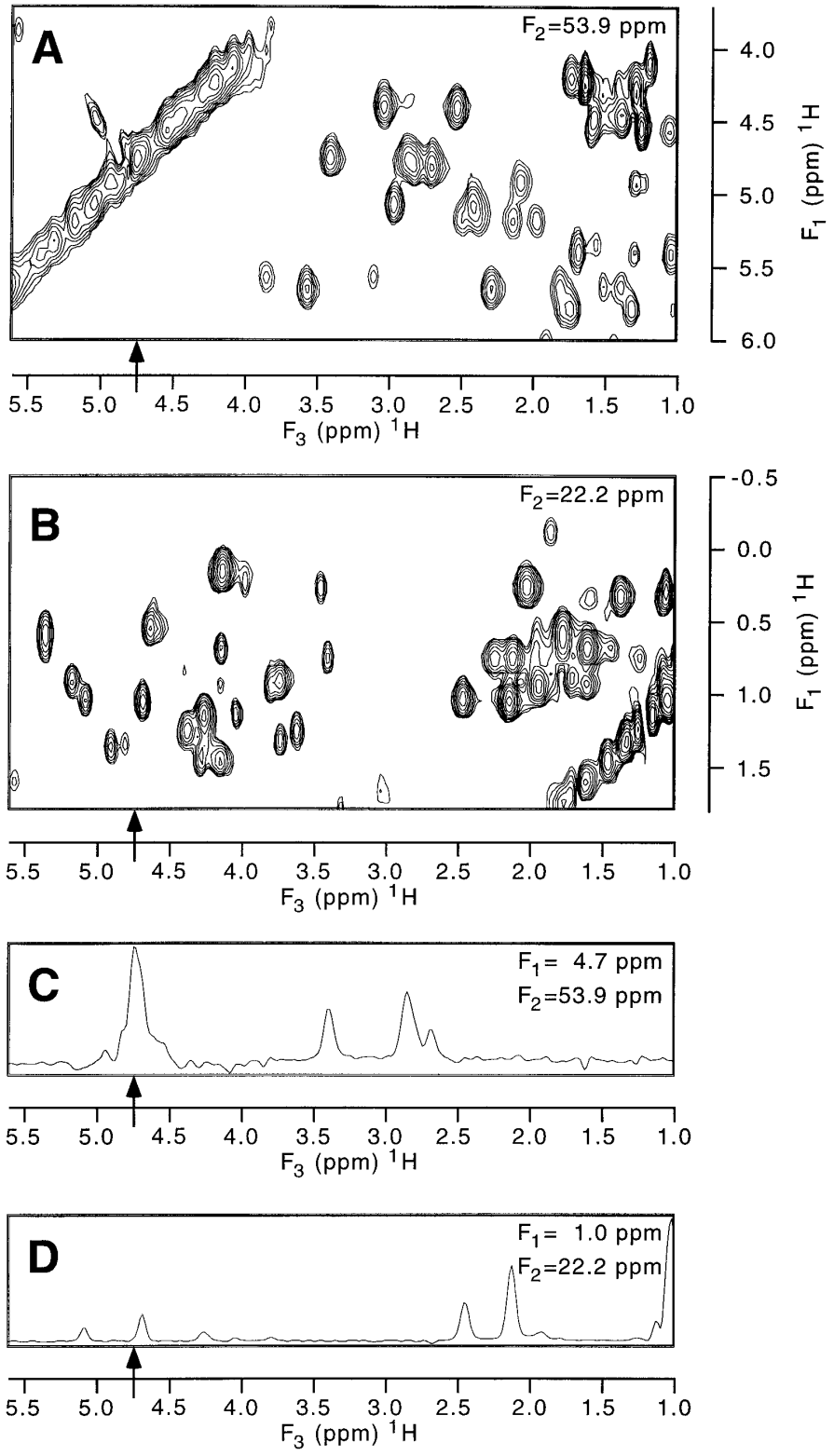
A
F2=53.9 ppm
4.0
4.5
5.0
5.5
6.0
F1 (ppm) 1H
5.5 5.0 4.5 4.0 3.5 3.0 2.5 2.0 1.5 1.0
F3 (ppm) 1H
B
F2=22.2 ppm
-0.5
0.0
0.5
1.0
1.5
F1 (ppm) 1H
5.5 5.0 4.5 4.0 3.5 3.0 2.5 2.0 1.5 1.0
F3 (ppm) 1H
C
F1= 4.7 ppm
F2=53.9 ppm
5.5 5.0 4.5 4.0 3.5 3.0 2.5 2.0 1.5 1.0
F3 (ppm) 1H
D
F1= 1.0 ppm
F2=22.2 ppm
5.5 5.0 4.5 4.0 3.5 3.0 2.5 2.0 1.5 1.0
F3 (ppm) 1H

FIGURE 3

eTOCSY–eCP sequence, we recorded $^{13}C-^{1}H$ planes with both the unenhanced and singly enhanced version of the pulse sequences, 1A and 1B, with $t_1 = 0$. The planes are shown in Figs. 2A and Fig. 2B, respectively. As discussed, a signal-to-noise ratio improvement of $2^{1/2}$ is expected. Indeed, the enhancement is significant as can be seen upon comparison of Figs. 2A and 2B. To establish the additional enhancement by also incorporating the eCP sequence, we show in Fig. 2C and Fig. 2D the $^{1}H-^{1}H$ planes recorded with the singly and doubly enhanced versions of the pulse sequences, 1B and 1C, respectively, with $t_2 = 0$. Again, as discussed, a signal-to-noise ratio improvement of $2^{1/2}$ is expected. As can be seen, the enhancement is considerable.

A few comments should be made. (1) As has been shown by Schleucher *et al.* (*14*) both the eINEPT and the eCP sequences do not achieve optimum sensitivity enhancement for CH and CH_2 multiplicities simultaneously. The eCP sequence gives optimum sensitivity for CH moieties when the CP mixing time, τ_m, equals $1/J_{CH}$ and for CH_2 moieties when τ_m equals 0.7 $(1/J_{CH})$. We have chosen an intermediate value, $\tau_m \approx 0.85\ (1/J_{CH})$. As can be seen (see Figs. 2A and 2B), this setting leads to significant enhancement of cross peaks involving either α or β protons. (2) To achieve the highest enhancement factors, we observed that it is better to keep the length of the additional delay periods as short as possible than to optimize the length of τ_m. (3) The presented doubly enhanced CP HCCH–TOCSY experiment (Fig. 1C) is simple and easy to set up as compared to the INEPT-based HCCH–TOCSY experiment. For example, the required length of τ_m $[\approx 0.85(1/J_{CH})]$ dictates the 90° ^{1}H and ^{13}C pulse lengths to be both approximately 26.7 μs, and thereby determines the corresponding radiofrequency field strengths required for Hartman–Hahn matching. Although optimization of the power settings was found to be advantageous, considerable signal was already obtained at roughly the correct pulse lengths.

An important additional feature of the doubly enhanced 3D CP HCCH–TOCSY experiment is the extremely good water suppression. This is already evident from Figs. 2, but becomes even more striking when considering the doubly enhanced 3D CP HCCH–TOCSY spectrum. Figure 3 demonstrates the latter. We selected a $^{1}H-^{1}H$ plane at an F_2 frequency of α carbons (Fig. 3A), in which several of the directly bonded protons resonate at the water resonance frequency ($F_3 = 4.7$ ppm). The diagonal cross peak at the water frequency, which represents nontransferred magnetization, i.e., $H_\alpha \rightarrow C_\alpha \rightarrow H_\alpha$, is quite clearly visible. In addition, genuine cross peaks which resonate close to or at the water frequency, for instance, those representing the transfer route $H_\beta \rightarrow C_\beta \rightarrow H_\alpha$, are also clearly visible (Fig. 3B). The F_3 1D slices through these resonances, as shown in Figs. 3C and 3D, respectively, highlight the minimal baseline distortions observed.

To achieve such an excellent degree of water suppression, we investigated and tested various aspects of this suppression. Using sequence 1A without water presaturation, we were not able to obtain consistently good water suppression, even with considerable gradient lengths and strengths, and/or with low-field continuous-wave irradiation during the homonuclear carbon TOCSY period (*7*). Ultimately, the best result, as shown in Fig. 2A, was obtained using a weak presaturation field. Consistently better water suppression was obtained using the singly and doubly enhanced sequences, 1B and 1C, respectively. Now, however, the strengths and lengths of the gradients employed did affect the quality of the water suppression. Very good water suppression was obtained with the settings as given in the legend to Fig. 3. Weaker and shorter gradients also resulted in good suppression but not in a consistent manner; i.e., the water suppression was excellent for a number of scans, but occasionally a single free-induction decay with poor suppression appeared. In the latter circumstances, presaturation did not improve the water suppression, nor did the inclusion of a weak irradiating field during the homonuclear ^{13}C DIPSI-3 sequence as suggested by Wang and Zuiderweg (*7*), nor the inclusion of a water flip-back pulse positioned just prior to the first gradient in sequence 1B. We observed that the quality of the shimming also affects the quality of the water suppression, i.e., poorer shimming required stronger gradients. This is confirmed by Czisch *et al.* (*17*) who recently reported a systematic study of the effects of shimming on the water signal suppression. Well-shimmed samples give improved water suppression. This may also explain why we observed that acquisition of spectra using two different probes required different gradient settings (of about a factor of two in length) to achieve good water suppression.

Based on the aforementioned experiences and on the observation that stronger and longer gradients cause decreased sensitivity, we arrived at the following protocol for obtaining high sensitivity and good water suppression in a 3D CP HCCH–TOCSY experiment. The sequence and the gradient settings as given in the legend to Fig. 3 should be used as a starting point. Choose gradients two and three in sequence 1C to be initially rather weak and short (start with about half the values as given in the legend to Fig. 3). Then the length and strength of the second and third gradients should systematically be increased, while maintaining coherence selection by properly adjusting the strength and/or length of the first and final gradients, until consistently good water suppression is obtained for each individual FID.

In conclusion, we have demonstrated the implementation of singly and doubly enhanced 3D CP HCCH–TOCSY experiments. In both experiments, gradients are used for coherence selection and heteronuclear cross polarization is used to achieve both $^{1}H \rightarrow {}^{13}C$ and $^{13}C \rightarrow {}^{1}H$ magnetization transfer. The experiments are easy to set up and produce high quality spectra of ^{13}C-labeled proteins in H_2O solution. They are characterized by excellent water suppression, and show

improved sensitivity as compared to the sensitive-unenhanced version of the experiment. The 3D CP HCCH–TOCSY experiments presented eliminate the need to acquire these experiments in D_2O. A practical protocol to achieve excellent water suppression has been given. The latter is of importance since we found that the exact gradient settings depend somewhat on the probe used and the quality of its shimming.

ACKNOWLEDGMENTS

This work was supported by the Dutch Foundation for Chemical Research (SON). Spectra were recorded at the SON/NWO National HF-NMR Facility (Nijmegen, The Netherlands) supported by SON. The research of Carlo P. M. van Mierlo has been made possible by a fellowship of the Royal Netherlands Academy of Arts and Sciences. H. Janssen of Bruker Spectrospin (The Netherlands) provided the unix script which could be modified to conveniently record the doubly enhanced 3D CP HCCH–TOCSY spectrum.

REFERENCES

1. A. Bax and S. Grzesiek, *Acc. Chem. Res.* **26,** 131 (1993).
2. A. S. Edison, F. Abildgaard, W. M. Westler, E. S. Mooberry, and J. L. Markley, ''Methods in Enzymology'' (T. L. James and N. J. Oppenheimer, Eds.), Vol. 239, p. 3, Academic Press, San Diego, 1994.
3. A. Bax, G. M. Clore, and A. M. Gronenborn, *J. Magn. Reson.* **88,** 425 (1990).
4. S. W. Fesik, H. L. Eaton, E. T. Olejniczak, E. R. P. Zuiderweg, L. P. McIntosh, and F. W. Dahlquist, *J. Am. Chem. Soc.* **112,** 886 (1990).
5. E. R. P. Zuiderweg, *J. Magn. Reson.* **89,** 533 (1990).
6. A. Majumdar, H. Wang, R. C. Morshauser, and E. R. P. Zuiderweg, *J. Biomol. NMR* **3,** 387 (1993).
7. H. Wang and E. R. P. Zuiderweg, *J. Biomol. NMR* **5,** 207 (1995).
8. L. E. Kay, *Curr. Opin. Struct. Biol.* **5,** 674 (1995).
9. L. E. Kay, P. Keifer, and T. Saarinen, *J. Am. Chem. Soc.* **114,** 10663 (1992).
10. M. Sattler, M. G. Schwendinger, J. Schleucher, and C. Griesinger, *J. Biomol. NMR* **6,** 11 (1995).
11. M. Sattler, P. Schmidt, J. Schleucher, O. Schledetzky, S. J. Glaser, and C. Griesinger, *J. Magn. Reson. B* **108,** 235 (1995).
12. V. V. Krishnamurthy, *J. Magn. Reson. B* **106,** 170 (1995).
13. S. S. Wijmenga, C. P. M. van Mierlo, and E. Steensma, *J. Biomol. NMR* **8,** 319–330 (1996).
14. J. Schleucher, M. Schwendinger, M. Sattler, P. Schmidt, O. Schedletzky, S. J. Glaser, O. W. Sørensen, and C. Griesinger, *J. Biomol. NMR* **4,** 301 (1994).
15. J. Keeler and D. Neuhaus, *J. Magn. Reson.* **63,** 454 (1985).
16. F. J. M. van de Ven, ''Multidimensional NMR in Liquids'', p. 71, VCH, Cambridge, 1995.
17. M. Czisch, A. Ross, C. Cieslar, and T. A. Holak, *J. Biomol. NMR* **7,** 121 (1996).
18. A. J. Shaka, C. J. Lee, and A. Pines, *J. Magn. Reson.* **77,** 274 (1988).
19. D. Marion, M. Ikura, R. Tschudin, and A. Bax, *J. Magn. Reson.* **85,** 393 (1989).
20. A. J. Shaka, P. B. Barker, and R. Freeman, *J. Magn. Reson.* **64,** 547 (1985).